ACS Macro Letters

Letter

pubs.acs.org/macroletters

Inverse Design of Topographical Templates for Directed Self-Assembly of Block Copolymers

Adam F. Hannon,* Kevin W. Gotrik, Caroline A. Ross, and Alfredo Alexander-Katz*

Department of Materials Science and Engineering, Massachusetts Institute of Technology, Cambridge, Massachusetts 02139, United States

ABSTRACT: A computational inverse design algorithm is presented that predicts the necessary topographical template to direct the self-assembly of a diblock copolymer thin film into a desired complex morphology. This topographical template is determined from the spatial configuration of a template that results in an energy minimum for the system. Degenerate solutions are accounted for by performing multiple simulations with random starting configurations of the topographical template and making a statistically weighted template that is tested using self-consistent field theory simulations. The final template is, thus, the inverse design solution of the desired block copolymer morphology. The results also yield nonintuitive post-configuration design principles.

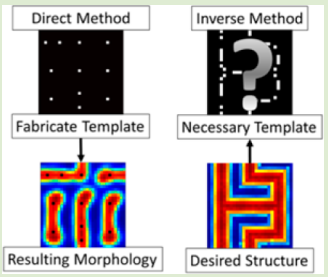

The continuing miniaturization of microprocessors and memory has enabled a technological revolution over the last several decades, but the reduction in feature size of these devices requires continued development of nanofabrication techniques. Traditional photolithography based on 193 nm wavelength light is limited to defining features with period of order 40 nm, and accessing sub-20 nm feature sizes requires new approaches. One of the techniques to reach these length scales is the directed self-assembly of thin film block copolymers to form arrays of nanoscale microdomains by microphase separation.[1] The microdomains from patterns of dots, lines, and other features can be used as a mask for pattern transfer.

Directed self-assembly of block copolymer films using templates consisting of chemical or topographical features has allowed for the formation of patterns of lines and dots with long-range order.[2−7] However, obtaining aperiodic features such as bends, junctions, or isolated features remains a key challenge and has so far only been demonstrated empirically using relatively simple template designs.[8−10] For example, templates such as round and elliptical posts with different chemical functionalization produced a range of microdomain geometries.[11] These templated self-assembly results have been successfully reproduced using self-consistent field theory (SCFT) in which field boundary conditions modeled the experimental topographical or chemical template features.[12−25] In all these calculations, however, the starting point is defining the template and then one calculates the resulting microdomain morphology; that is, they solve the "forward" problem.

In this study, we demonstrate an algorithm that uses a random optimization process in combination with SCFT simulations to solve the "inverse" design problem of block copolymer directed self-assembly. In other words, we use the algorithm to determine the topographical template needed to direct the block copolymer self-assembly to form a predetermined target pattern. This procedure eliminates the need to scan the large parameter space of potential template geometries and is particularly relevant to lithographic applications in which the final pattern is known but the template unknown.

The inverse self-assembly problem has been explored in other self-assembling systems, such as the case of colloids investigated by Torquato et al.[26,27] to determine the intercolloid potential that ensures that the free energy minimum state has a particular symmetry. For block copolymers, there has been very limited study of the inverse problem apart from recent work on determining the templates required for making contact vias and bends in specific locations.[28−31] Solving the inverse problem for block copolymer self-assembly is particularly useful, not just for nanolithography applications, but for inverse design studies in general because it is possible to synthesize the materials and templates in an efficient manner, rendering the solutions feasible to implement and test, and potentially enabling extension to create tailored hierarchical and heterogeneous mesoscale materials.

The inverse design problem is based on modeling a template consisting of topographical posts with diameter d and height h, which correspond to experimental posts formed from resist materials such as hydrogen silsequioxane (HSQ) or carbonized poly(methyl methacrylate) (PMMA) made using electron beam lithography.[21−24] The posts were modeled using a large hard wall potential prohibiting the polymer density from occupying the grid points corresponding to the posts, resulting in total polymer density in these regions less than ∼0.1. The model parameters included the Flory−Huggins parameter χ, degree of polymerization N, and volume fraction of the minority component f. The modeling described here corresponded to a 45.5 kg/mol f_{PDMS} = 33.5% poly(styrene-

Received: January 28, 2013
Accepted: February 27, 2013
Published: March 5, 2013

b-dimethylsiloxane) (PS-PDMS) block copolymer that forms cylindrical morphologies in bulk, which has been explored in detail.[23,24] For the initial demonstration of the method, 2D simulations were performed, and to model in-plane cylinders a volume fraction of $f = 0.44$ was used in the simulations. χN was set to a value of 14 to reflect an effective value for the system in a solvent annealing environment. The posts had an additional field constraint around their perimeter to make them attractive to one block and repulsive to the other to model brush layer coatings corresponding to densities at the post wall of ~0.9 of the attracted block.

Here we outline the steps of the algorithm that was used to obtain the inverse solution template for a given target microdomain morphology in 2D. These steps are shown with results for an example target structure in Figure 1.

The block copolymer morphology is characterized by the density field solutions ϕ_A and ϕ_B in the SCFT simulations for the two blocks, *A* and *B* (for information on how these SCFT simulations are performed, see Supporting Information in ref 21, as well as refs 32 and 33).[21,32,33] We first describe how target structures were initiated in the simulations. The desired field structure was built up from "primitive cells" of dimensions approximately L_0 by L_0, where L_0 is the natural period of the block copolymer. The density fields in the primitive cells were solved using the SCFT equations. Each primitive cell was on an N_x by N_y grid (9 × 9 grid points at a coarse-graining of about ~4 nm length per 1 grid point). The target structure density was then built up by concatenating these primitive cells using various symmetry operations to create bends, junctions, and hole structures characteristic of the desired functional device pattern. We tested the method with a target structure that contained four 90° bends, two three-way junctions, and straight segments with periodic boundary conditions as shown in Figure 1a.

The target field configuration was seeded with a fixed number of template posts N_{posts} in a random spatial configuration. $N_{posts} = 24$ was selected with the posts preferential to the minority block *A*. The number of posts was chosen to reflect a reasonable density of template features corresponding to between 2 and 3 posts per L_0 by L_0 primitive cell in this example. The posts in this study had a fixed size of 3 × 3 grid points in which the center grid point had a large compressibility field $i\Omega_+ = -20$ to model the physical post and the surrounding 8 grid points were attractive to either the *A* or *B* polymer to model the brush layer with $\Omega_- = \pm 5$. Here $i\Omega_+$ and Ω_- are the pressure-like and exchange chemical potential fields respectively. Random configurations were used rather than a guessed solution to ensure the algorithm was not biased and multiple simulations could be compared.

Once the target density was initialized, the inverse algorithm proceeded in the following fashion. A normal SCFT simulation was performed holding the target structure densities constant while relaxing the chemical potential fields using a complex Langevin scheme for sufficient iterations to reach the steady state solution. Once this steady state was reached, the free energy *H* was calculated.[21,32,33] Here *H* is given by

$$\frac{H}{kT} = \frac{\rho_0 R_g^3}{N}\left(\int\left((2f-1)\Omega_- + \frac{1}{\chi N}\Omega_-^2 - i\Omega_+\right)d\vec{r} - V\ln Q\right)$$

where ρ_0 is the monomer density, R_g is the radius of gyration, *N* is the degree of polymerization, χ is the Flory–Huggins interaction parameter, *f* is the volume fraction, *V* is the grid volume, $\vec{r}$ is the spatial coordinate, and *Q* is the single chain partition function.

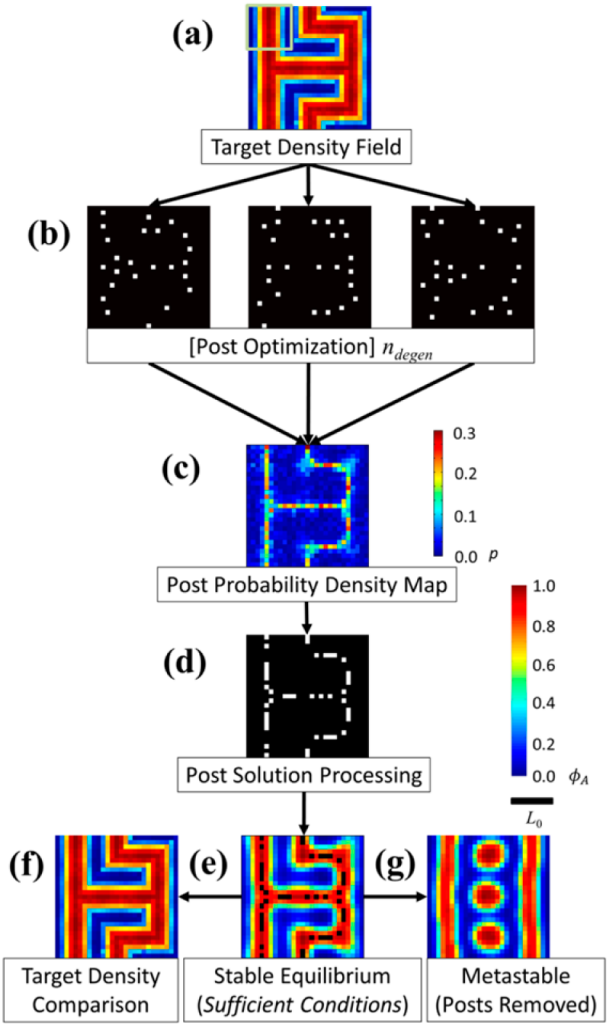

Figure 1. Outline of steps in the inverse algorithm with results for a given target structure containing bends and three-way junctions. Scale bar with length L_0 and the ϕ_A color bar are shown to the right of d. (a) Density field of target structure initialization. Red represents $\phi_A = 1$ for the minority block. Green square highlights a single primitive cell. (b) Three post configurations from three separate simulations found during $n_{degen} = 150$ inverse algorithm simulations. (c) Probability density map *p* found by summing the post positions over $n_{degen} = 150$ solutions and normalizing. Color bar for *p* is shown to the right. (d) Weighted inverse solution with symmetry considerations for the system considering $p_{thresh} = 0.20$. (e) Density fields using the inverse solution post configuration with random initial conditions showing the stable equilibrium solution found satisfies the *sufficient conditions* of an inverse design solution. (f) Original target density structure for comparison with result from e. (g) Density field result calculated by taking posts out of the system in e and letting the system relax shows the posts are necessary for the target structure to be stable.

Starting in a predetermined order, the posts were moved one at a time in a random walk. The posts were prohibited from overlapping each other using a hard sphere assumption condition. After a post was moved, a constrained density SCFT simulation was run and the resulting energy calculated and compared to the previous free energy. If the new configuration was lower in free energy, the post configuration was accepted and the algorithm moved to the next post. If the

dx.doi.org/10.1021/mz400038b | *ACS Macro Lett.* 2013, 2, 251–255

free energy was higher, the post was moved in another random walk step. If after n_{move} steps a lower free energy configuration had not been found, the algorithm put the post back to its previous starting position and the next post underwent the random walk minimization. This sequence was performed for all posts n_{scan} times. For the target structure considered, n_{move} = 20 and n_{scan} = 5; however, these parameters can be further optimized for algorithm efficiency. Once complete, the lowest energy configuration of posts found was accepted as a candidate inverse solution. A plot of H normalized by kT over the course of a simulation is shown in Figure 2. The final field structure with this post configuration was then relaxed to ensure the solution satisfied the *necessary conditions* required for an inverse solution.

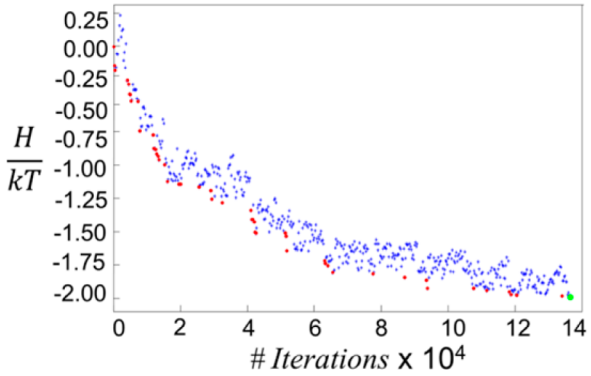

Figure 2. Normalized free energy H/kT vs iterations for a single inverse algorithm for the target structure examined in Figure 1. Red points designate points in the simulation where a new post configuration was accepted with lower energy. The green point represents the lowest energy configuration observed during the simulation. # Iterations account for individual SCFT field relaxation steps with 250 of these corresponding to a single data point.

Block copolymer systems are known for exhibiting multiple metastable or degenerate morphologies for a given set of boundary conditions. Conversely, for some target structures, multiple post configurations may yield nearly the same final structure within the required specifications. To account for these facts, the inverse algorithm was performed n_{degen} times for a given target structure then a statistical weighted sampling of the resulting post locations in the candidate solutions was calculated to produce the inverse solution. Once energy minimum configurations were found for the n_{degen} simulations, the final template configuration was made by summing over the n_{degen} post locations. The inverse algorithm was performed for n_{degen} = 150 times for the target structure. Examples of three of the final post configurations from the 150 trials are shown in Figure 1b. For these configuration, the calculated value of H/kT was on average −1.99, with a standard deviation of 0.24 indicating the different solutions were spread in terms of energy.

For the post-arrangements produced in each simulation, the target density constraint was removed and the structure was allowed to relax to demonstrate that with the posts the solution produced a morphology that approximately matched the target density structure. This demonstrated the *necessary condition* that the template was the inverse solution of the target structure.

The summing and normalizing by n_{degen} resulted in a probability map p that showed the most likely positions for the posts in the inverse solution template. This probability density map is shown in Figure 1c. Post locations for the final inverse solution template were chosen by only keeping posts in positions with probability p greater than a threshold probability p_{thresh}.

Using the probability density map template structure, an averaged inverse solution was created with a p_{thresh} = 0.20 for the target structure. This value for p_{thresh} was chosen such that the system had ∼24 posts. The post template solution was then made symmetrical to match the symmetry of the final target pattern. Because the target structure was mirror-symmetric, posts were added to the solution to ensure mirror symmetry, Figure 1d. This symmetry consideration resulted in the final system having closer to 40 total posts as well as some posts neighboring each other. The resulting template solution was considered to be an inverse design solution.

To demonstrate that the template satisfied the *sufficient condition* that the template yielded the target density fields upon initializing the simulation with a random field seeding, several simulations were performed after randomly initializing the template. This template was then used in a forward SCFT relaxation simulation with random initial field conditions to calculate the equilibrium solution for the block copolymer density fields, Figure 1e, which can be compared with the target structure in Figure 1f.

After comparing the final resulting density fields to the target density fields and observing a match, the template was deemed to be an inverse solution for the given target structure. The final structure matches well with the target structure. Additionally, relaxing this density field solution with the posts removed demonstrated that without the posts the solution would not be stable, Figure 1g.

In addition to giving a template that fulfills the *necessary and sufficient conditions* needed for an inverse design solution for block copolymer directed self-assembly, the inverse algorithm demonstrated here gives insight into template design features that are nonintuitive from empirical design. One might expect for the case when posts are preferential to the minority block, to produce sharp bends the posts would be concentrated in the center of the bend to guide the minority microdomain around the bend. Similarly, to form a three-way junction, a T-shaped post may be expected, as depicted in Figure 3a. However, the inverse design simulations showed that post positions in the center of the junction or bend were in fact less likely, and instead the posts were located as shown in Figure 3b. Therefore, intuitive "connect-the-dots" strategies do not necessarily produce the desired results. Furthermore, the final morphology may contain unanticipated features. For the square ring-shaped target structure shown in Figure 3c, additional circular minority microdomains such as those shown in Figure 3d were produced at the corners of the simulation. This can be avoided by using instead posts that are attractive to the majority block, illustrated in Figure 3e.

The inverse algorithm as presented thus far is by no means optimal nor are the solutions found necessarily unique. As a demonstration, additional simulations of the target structure from Figure 1 were done to increase n_{degen} from 150 up to 2100. This had the result of making the post probability map more symmetrical. To maintain ∼24 posts, a new p_{thresh} = 0.29 was selected. In the solution, there were only a couple of posts that did not conform to the mirror symmetry of the target structure. These nonmirrored posts were eliminated from the structure leaving exactly 24 posts. Testing this resulting

dx.doi.org/10.1021/mz400038b | ACS Macro Lett. 2013, 2, 251−255

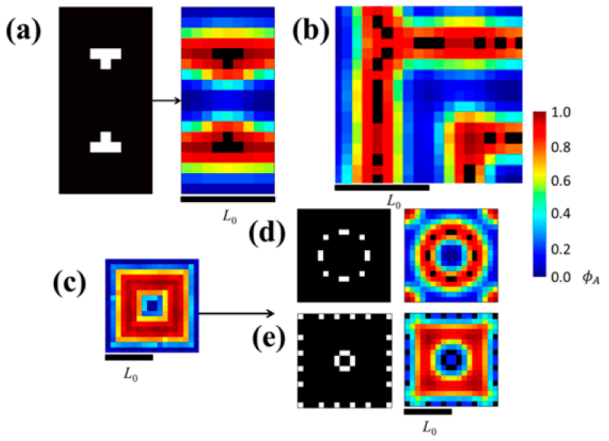

Figure 3. Nonintuitive template design feature. ϕ_A color bar is shown to the right. (a) Left: Empirical guess solution for making three-way junctions. Right: The T-shaped posts did not stabilize the junctions but instead only formed strained lamellae. (b) A nonintuitive post configuration required to form a three-way junction and a 90° bend deduced from the inverse algorithm. (c) Target structure containing only a square ring-shaped structure with four 90° bends. (d) Left: The best inverse solution found using minority-preferential posts. Right: The resulting morphology, which formed an additional microdomain at the corners of the simulation. (e) Left: The best inverse solution found using majority-preferential posts. Right: The resulting morphology, which formed the target structure accurately.

structure yielded an acceptable structure that met the *necessary and sufficient* conditions for the inverse design solution. The resulting solution is compared with the original solution and their resulting density fields in Figure 4.

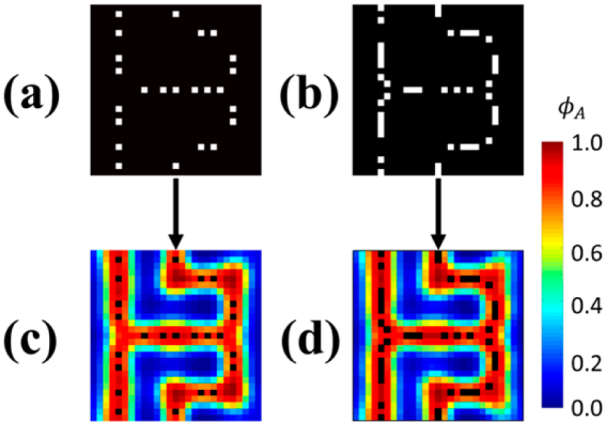

Figure 4. Comparison of inverse solution results for target structure in Figure 1. (a) Inverse solution for n_{degen} = 2100, where the symmetry of the target pattern is produced in the probability map. (b) Inverse solution for n_{degen} = 150 in which additional posts were added to account for the symmetry of the target pattern. (c) Forward SCFT density profile for n_{degen} = 2100. (d) Forward SCFT density profile for n_{degen} = 150 plus symmetry consideration.

These results demonstrate that in target structures with symmetry, it is possible to save computation time by using a lower n_{degen} and imposing symmetry on the resulting probability map, but a symmetric solution can also be produced without postprocessing if n_{degen} is sufficiently high. The reason n_{degen} must be so large to obtain the expected symmetry is due to the random noise introduced in the field relaxation scheme that breaks the symmetry of the structure, so locations that have p nearly equal to p_{thresh} will vary compared to their mirrored counterpart. In other words, the posts at locations corresponding to $p \approx p_{thresh}$ are not the most important ones in determining the structure, so their presence or absence does not greatly promote or inhibit the formation of the target structure. This reinforces the observation that there is not a single unique inverse solution for a given target structure.

In summary, an inverse design method for topographical templating of block copolymer morphologies has been demonstrated computationally. The method calculates the necessary template for the directed self-assembly of a specific target block copolymer morphology assuming the target is an equilibrium structure under the topographical constraints imposed. The method was verified computationally through traditional SCFT simulations with field boundary condition constraints modeling the topographical features. Nonintuitive post templating design rules are derived from the resulting templates.

The algorithm has room for optimization including initializing the simulation with guessed solutions rather than random solutions, increasing the n_{scan} and n_{move} parameters to a value that converges more quickly to a minimum energy configuration, using combinations of majority and minority preferential posts for a more general solution, moving multiple posts at the same time, and using less coarse-graining with more detailed posts that better model the experimental post geometry, including extension to 3D. However, the approach presented here demonstrates that such algorithms can be used to predict templates for complex layouts with utility in lithographic applications.

AUTHOR INFORMATION

Corresponding Author

*E-mail: aalexand@mit.edu; thefloyd@mit.edu.

Notes

The authors declare no competing financial interest.

ACKNOWLEDGMENTS

We gratefully acknowledge financial support from the National Science Foundation Award #1246740, Taiwan Semiconductor Manufacturing Company, and Semiconductor Research Corporation.

REFERENCES

(1) Segalman, R. A. *Mater. Sci. Eng., R* **2005**, *48*, 191−226.
(2) Kim, S. O.; Solak, H. H.; Stoykovich, M. P.; Ferrier, N. J.; de Pablo, J. J.; Nealey, P. F. *Nature* **2003**, *424*, 411−414.
(3) Cheng, J. Y.; Ross, C. A.; Smith, H. I.; Thomas, E. L. *Adv. Mater.* **2006**, *18*, 2505−2521.
(4) Bita, I.; Yang, J. K. W.; Jung, Y. S.; Ross, C. A.; Thomas, E. L.; Berggren, K. K. *Science* **2008**, *321*, 939−943.
(5) Ruiz, R.; Kang, H.; Detcheverry, F. A.; Dobisz, E.; Kercher, D. S.; Albrecht, T. R.; de Pablo, J. J.; Nealey, P. F. *Science* **2008**, *321*, 936−939.
(6) Detcheverry, F. A.; Nealey, P. F.; de Pablo, J. J. *Macromolecules* **2010**, *43*, 6495−6504.
(7) Ruiz, R.; Dobisz, E.; Albrecht, T. R. *ACS Nano* **2011**, *5*, 79−84.
(8) Stoykovich, M. P.; Müller, M.; Kim, S. O.; Solak, H. H.; Edwards, E. W.; de Pablo, J. J.; Nealey, P. F. *Science* **2005**, *308*, 1442−1446.
(9) Stoykovich, M. P.; Kang, H.; Daoulas, K. C.; Liu, G.; Liu, C.-C.; de Pablo, J. J.; Müller, M.; Nealey, P. F. *ACS Nano* **2007**, *1*, 168−175.
(10) Kim, S. O.; Kim, B. H.; Meng, D.; Shin, D. O.; Koo, C. M.; Solak, H. H.; Wang, Q. *Adv. Mater.* **2007**, *19*, 3271−3275.

(11) Yang, J. K. W.; Jung, Y. S.; Chang, J.-B.; Mickiewicz, R. A.; Alexander-Katz, A.; Ross, C. A.; Berggren, K. K. *Nat. Nanotechnol.* **2010**, *5*, 256−260.
(12) Thompson, R. B.; Ginzburg, V. V.; Matsen, M. W.; Balazs, A. C. *Science* **2001**, *29*, 2469−2472.
(13) Thompson, R. B.; Ginzburg, V. V.; Matsen, M. W.; Balazs, A. C. *Macromolecules* **2002**, *35*, 1060−1071.
(14) Yu, B.; Sun, P.; Chen, T.; Jin, Q.; Ding, D.; Li, B.; Shi, A.-C. *Phys. Rev. Lett.* **2006**, *96*, 138306−1−4.
(15) Yu, B.; Sun, P.; Chen, T.; Jin, Q.; Ding, D.; Li, B.; Shi, A.-C. *J. Chem. Phys.* **2007**, *126*, 204903−1−5.
(16) Kriksin, Y. A.; Neratova, I. V.; Khalatur, P. G.; Khokhlov, A. R. *Chem. Phys. Lett.* **2010**, *492*, 103−108.
(17) Tang, Q.; Ma, Y. *Soft Matter* **2010**, *6*, 4460−4465.
(18) Hur, S.-M.; Garcia-Cervera, C. J.; Kramer, E. J.; Fredrickson, G. H. *Macromolecules* **2009**, *42*, 5861−5872.
(19) Mishra, V.; Fredrickson, G. H.; Kramer, E. J. *ACS Nano* **2012**, *6*, 2629−2641.
(20) Takahashi, H.; Laachi, N.; Hur, S.-M.; Wienheimer, C. J.; Shykind, D.; Fredrickson, G. H. *Proc. SPIE* **2012**, *8323*, 83231N-1−6.
(21) Mickiewicz, R. A.; Yang, J. K. W.; Hannon, A. F.; Jung, Y. S.; Alexander-Katz, A.; Berggren, K. K.; Ross, C. A. *Macromolecules* **2010**, *43*, 8290−8295.
(22) Chang, J.-B.; Son, J. G.; Hannon, A. F.; Alexander-Katz, A.; Ross, C. A.; Berggren, K. K. *ACS Nano* **2012**, *6*, 2071−2077.
(23) Tavakkoli, K.G., A.; Gotrik, K. W.; Hannon, A. F.; Alexander-Katz, A.; Ross, C. A.; Berggren, K. K. *Science* **2012**, *336*, 1294−1298.
(24) Tavakkoli, K.G., A.; Hannon, A. F.; Gotrik, K. W.; Alexander-Katz, A.; Ross, C. A.; Berggren, K. K. *Adv. Mater.* **2012**, *24*, 4249−4254.
(25) Hardy, C. G.; Tang, C. *J. Polym. Sci., Part B: Polym. Phys.* **2013**, *51*, 2−15.
(26) Torquato, S. *Soft Matter* **2009**, *5*, 1157−1173.
(27) Cohn, H.; Kumar, A. *Proc. Natl. Acad. Sci. U.S.A.* **2009**, *106*, 9570−9575.
(28) Yi, H.; Bao, X.-Y.; Zhang, J.; Bencher, C.; Chang, L.-W.; Chen, X.; Tiberio, R.; Conway, J.; Dai, H.; Chen, Y.; Mitra, S.; Wong, H.-S. P. *Adv. Mater.* **2012**, *24*, 3107−3114.
(29) Seino, Y.; Yonemitsu, H.; Sato, H.; Kanno, M.; Kato, H.; Kobayashi, K.; Kawanishi, A.; Azuma, T.; Muramatsu, M.; Nagahara, S.; Kitano, T.; Toshima, T. *Proc. SPIE* **2012**, *8323*, 83230Y-1−7.
(30) Hinsberg, W.; Cheng, J.; Kim, H.-C.; Sanders, D. P. *Proc. SPIE* **2010**, *7637*, 76370G-1−11.
(31) Doerk, G. S.; Liu, C.-C.; Cheng, J. Y.; Rettner, C. T.; Pitera, J. W.; Krupp, L. E.; Topuria, T.; Arellano, N.; Sanders, D. P. *ACS Nano* **2013**, *7*, 276−285.
(32) Fredrickson, G. H. *The Equilibrium Theory of Inhomogeneous Polymers*; Oxford University Press: Oxford, England, 2006.
(33) Fredrickson, G. H.; Ganesan, V.; Drolet, F. *Macromolecules* **2002**, *35*, 16−39.